Catal Lett (2009) 131:612–617
DOI 10.1007/s10562-009-0015-y

Mechanism of Charge Transfer in the Transition Metal Ion Doped TiO_2 with Bicrystalline Framework of Anatase and Rutile: Photocatalytic and Photoelectrocatalytic Activity

L. Gomathi Devi · Nagaraju Kottam · S. Girish Kumar · K. S. Anantha Raju

Received: 1 April 2009 / Accepted: 29 April 2009 / Published online: 22 May 2009

Abstract The high photocatalytic activity of the Mn^{2+} doped TiO_2 with bicrystalline framework of anatase and rutile is probed for the degradation of benzene under solar light with/without applied bias. The enhanced activity is attributed to the transfer of electrons from the rutile to electron trapping/lattice trapping sites of anatase and also to the impurity level created by the dopant which favours effective charge separation. The shallow detrapping nature of Mn^{2+} dopant additionally contributes to the overall enhancement in the photocatalytic activity especially in the presence of applied electric field.

Keywords Manganese doped TiO_2 · Bicrystalline framework · Synergistic effect · Photoelectrocatalysis

1 Introduction

TiO_2 was doped with Mn^{2+} ion (Mn^{2+}–TiO_2) in order to investigate its influence on the phase transition and its photo catalytic activity was probed for the degradation of benzene with/without bias under solar light. Anatase TiO_2 was prepared by sol–gel technique [1]. Manganese oxalate [MnC_2O_4] was used as the source for Mn^{2+} ion. Calculated amount of anatase TiO_2 along with metal ion salt solution was added in order to get dopant concentration in the range of 0.02, 0.06 and 0.1% and labelled as T2, T3 and T4 respectively while the undoped TiO_2 is labelled as T1. The samples were calcined at 550^0 C for 4.5 h and were characterized by powder X-ray diffraction (PXRD), BET surface area measurements, UV-absorption and diffuse reflectance spectroscopy (DRS). The details of the analytical techniques used for the characterization and design of the photoreactor can be found elsewhere [2–4]. Photo electrocatalysis experiments are carried out with Princeton model 362 potentiostat. Both working and counter electrodes are platinum with a saturated calomel electrode (SCE) as a reference electrode. The experiments were carried out at various applied potentials +0.02, +0. 05, +0.1 and +0.20 V. Experiments using solar light (natural sun light) were carried out between 11 am to 2 pm during the summer season in Bangalore, INDIA. At this interval the fluctuation in solar intensity was minimal. The latitudes and longitudes are 12.58 N and 77.38 E, respectively. The average intensity of the sunlight is found to be around 1200 Wm^{-2}. The intensity of solar light was concentrated using a convex lens and the reaction mixture was exposed to this concentrated solar light. UV light source of 125 W capacity with a photon flux of 7.75 mW/cm^2 whose wavelength emission is in the range of 350–400 nm is used for comparative study. The reaction was stirred continuously over the entire time span of the experiment. At desired time intervals the samples were collected and centrifuged to separate the photocatalyst and were subjected to UV-Visible spectroscopic analysis using Shimadzu UV-1700 pharmaspec UV-visible spectrophotometer. To compare the photo catalytic activity of the above mentioned catalysts, the experiments were simultaneously conducted to avoid the error arising due to fluctuations in solar intensity. The photocatalytic efficiency was compared with commercially available Degussa P-25 TiO_2 (P25).

L. Gomathi Devi (✉) · N. Kottam · S. Girish Kumar · K. S. Anantha Raju
Department of Post Graduate Studies in Chemistry, Bangalore University, Central College City Campus, Dr. Ambedkar Street, Bangalore 560001, India
e-mail: gomatidevi_naik@yahoo.co.in

2 Results and Discussion

The PXRD patterns of Mn^{2+}–TiO_2 is shown in the Fig. 1. The samples T1 and T2 shows anatase phase while the samples T3 and T4 shows the bicrystalline framework of anatase and rutile. The rutile fraction increases with increase in the concentration of Mn^{2+} ions in the TiO_2 lattice. T3 shows higher anatase-to-rutile ratio of 90:10, while T4 shows higher rutile-to-anatase ratio of 52:48. These significant structural changes within the TiO_2 lattice were mainly due to the incorporation of Mn^{2+} ions. The ionic radius of Mn^{2+} (0.80 A°) is larger than the host Ti^{4+} ion (0.68 A°). The doping of substitutional metal cation with valancy less than +4 and with higher ionic size would induce oxygen vacancies at the surface of anatase crystallites favouring the bond rupture, ionic rearrangement and structure reorganisation for the formation of rutile phase [5]. Further the electrical imbalance between the dopant and host is maintained by inducing oxygen vacancies in the second co-ordination sphere. The oxygen vacancies induced by Mn^{2+} can be represented by Kroger-Vink notation [4];

$$MnO \leftrightarrow Mn''_{Ti} + Oo + Vo^{\cdot\cdot}/2Vo^{\cdot} \quad (1)$$

where $Vo^{\cdot}$ and $Vo^{\cdot\cdot}$ represents oxygen vacancies which are singly and doubly ionized. **Oo** is oxygen occupying oxygen lattice site. Mn $_{Ti}$ is manganese ion at titanium lattice site while the (′) represents the deficiency in the charge.

For the sample T2 with 0.02% Mn^{2+}, the induced oxygen vacancies are very few and may not facilitate rutile nucleation. With increase in the dopant concentration to 0.06% in the case of T3, the phase transition from anatase to rutile takes place at smoother rate and the phase transition rate is accelerated for higher dopant concentration (0.1%) in T4. The crystallite size calculated using Scherrer's equation is shown in the Table 1. The anatase crystallite size for the samples T1, T2, T3 and T4 are 26.2, 23.6, 20.3 and 16.6 nm, respectively, while the rutile crystallite size for the samples T3 and T4 were same as that of anatase. This result suggests that Mn^{2+} doping into the TiO_2 matrix effectively inhibit the grain growth of both the phases by providing dissimilar boundaries [6]. The powders with smaller crystallites will have large number of lattice defects. The defect sites on the surface of anatase crystallites react with sites in the neighbouring anatase crystal which may or may not possess defects favouring the formation of rutile nucleation at these sites. Further the atoms in the defect sites have higher energy than those in the main lattice and can favourably act as nucleation sites for the rutile phase formation at the surface of anatase crystallites. The decrease in crystallite size increases the total surface area due to the introduction of additional nucleation sites by the dopant. The higher rutile content for the sample T4 is mainly due to its smaller crystallite size which is believed to contain the higher density of surface defects on the anatase crystallite. Thus the high concentration of nucleation sites for the polymorphic phase transition from anatase to rutile exists at particle–particle interfaces in comparison to bulk materials. This might result in higher fraction of rutile for T4. The observed variation in the lattice parameter is the elongation of 'c' axis as shown in Table 1. Since only 'c' dimension is changing while 'a (=b)' remains almost constant for the range of dopant concentration, it can be concluded that Mn^{2+} substitutes Ti^{4+} ion preferentially on the bcc and fcc lattice in the anatase structure [7]. The shift in the band gap to the visible region was confirmed by UV-visible absorption spectroscopy. T3 showed maximum red shift of about 454 nm compared with T1 which showed strong absorption at 380 nm in the UV region (Fig. 2). The transition in T1 corresponds to band to band transition between O 2p levels (valence band) to Ti 3d levels (conduction band). Whereas in the case of T3, interband transitions arise between the impurity levels created by the dopant to the band gap states of bare TiO_2. The band gap values calculated from Kubelka Munk plot confirms the presence of impurity level around 0.5 eV below the conduction band edge of TiO_2 (Table 2).

T3 and P25 showed almost same photocatalytic activity under UV light, but under solar light T3 showed a better photocatalytic activity. The enhanced photocatalytic activity of T3 for the degradation of amaranth azo dye under solar light was previously reported by us [4]. However to confirm the role of dopant, we further carried out the degradation of 1 mL benzene (4.5 mg/250 mL) under solar

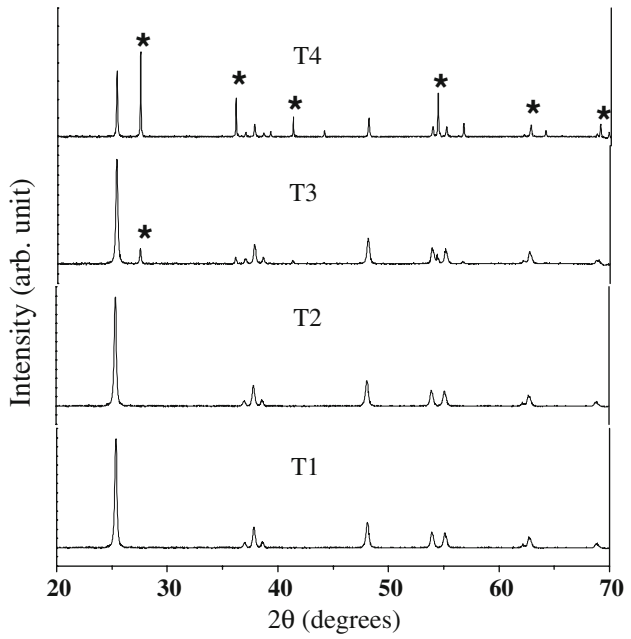

Fig. 1 PXRD patterns of Mn^{2+}–TiO_2 calcined at 550° C

Table 1 Diffraction peak of crystal plane (101) and d-spacing of crystal plane (101) of anatase, phase composition of anatase: rutile, lattice parameters, unit cell volume, and crystallite size of anatase (A):rutile (R)

Photo catalyst	2θ of crystal plane (101) of anatase	D-spacing of crystal plane (101) of anatase	Phase composition A:R	Lattice parameters A^0	Unit cell volume $(A^0)^3$	Crystallite size (nm) A:R
T1	25.32	3.50	100:0	a = b = 3.7828 c = 9.5023	135.97	26.2:0
T2	25.34	3.51	100:0	a = b = 3.7832 c = 9.5103	136.12	23.6:0
T3	25.36	3.51	90:10	a = b = 3.7824 c = 9.5211	136.21	20.3:20.3
T4	25.33	3.50	52:48	a = b = 3.7800 c = 9.5002	135.74	16.6:16.6

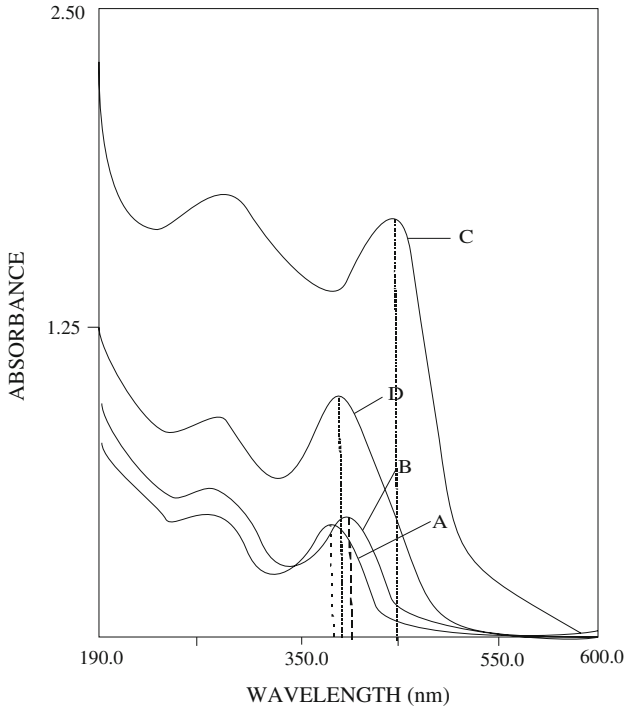

Fig. 2 UV-visible absorption spectra of all the photocatalysts.**a** T1, **b** T2, **c** T3, **d** T4

Table 2 Surface area, λ_{max} and band gap of all the photocatalysts

Photo catalyst	*Specific surface area (m^2/g)	λ_{max}	**Band gap
TiO_2 (T1)	18	380	3.2
Mn^{2+}(0.02%)–TiO_2 (T2)	21	426	2.9
Mn^{2+}(0.06%)–TiO_2 (T3)	26	454	2.7
Mn^{2+}(0.1%)–TiO_2 (T4)	24	420	2.9

* Specific surface area is measured from BET analysis

** Band gap was calculated from Kubelka Munk plot of $(1 - R_\infty)^2/2R_\infty$ versus wavelength

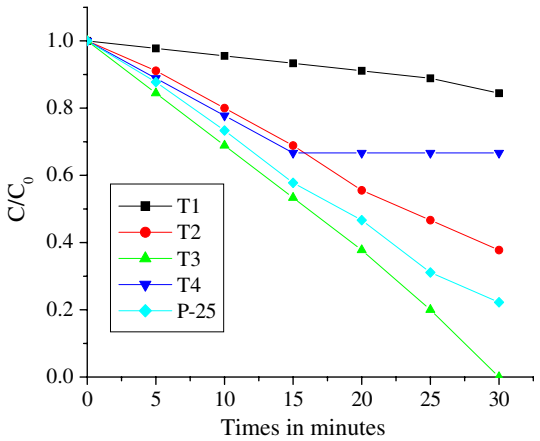

Fig. 3 Plot of C/C_0 versus time for the degradation of benzene under solar light

light. In addition, the mechanism for the charge transfer in T3 is compared with commercially available Degussa P-25 TiO_2 which also possess mixed phase. But in the case of T3, in addition to the mixed phases, it possesses electronic states created by the dopant. Figure 3 shows the plot of C/C_0 versus time for the degradation of benzene under solar light using all the photocatalysts and the corresponding first order rate constants are calculated. Though the variation of specific surface area of the doped catalysts is marginal, but the observed rate constant varied to a larger extent. The rate constant calculated for T2 (0.0345 min^{-1}) is almost four orders of magnitude higher than T4 (0.009 min^{-1}) despite the fact that both T2 and T4 had almost similar specific surface area. P25 with mixed phase showed enhanced activity (0.0484 min^{-1}) compared to T2 which had only anatase phase. Among the photocatalysts used, T3 (0.069 min^{-1}) shows enhanced activity suggesting the existence of synergistic effect due to the interaction between anatase and rutile crystallites. The activity of T3 was 1.4 times higher than P25 under solar illumination.

It is well known that this pair of polymorphs (anatase and rutile) can effectively reduce the recombination of photogenerated charge carriers to enhance the photocatalytic activity [8–20]. The band gap of rutile is favourable for visible light excitation as the conduction band edge of rutile lies below 0.2 eV compared to the conduction band edge of anatase. Under visible light excitation, the photogenerated electron from conduction band of rutile gets transferred to trapping sites of anatase phase. This can be considered as antenna effect by rutile phase. Subsequent transfer of electrons to lattice trapping sites of anatase further separates the charge carriers effectively. The lattice trapping sites of anatase are approximately located 0.8 eV below the conduction band edge of anatase [21]. These trapping sites prevent recombination to a large extent, thus facilitating the charge separation thereby activating the catalyst [22]. The hole originating from the rutile valence band participates in the oxidative degradation of organic pollutants. Similar charge transfer mechanism also takes place in T3. However, the sample T3 has an impurity dopant level at about $\approx$0.5 eV below the conduction band edge of anatase which is even lower than conduction band of rutile itself. Hence the electrons can easily be transferred to any of these three levels (Fig. 4).

The dopant Mn^{2+} ion has a unique stable half filled electronic configuration ($3d^5$). If it traps an electron it gets reduced to Mn^{+} and if it traps an hole it get oxidised to Mn^{3+}. According to crystal field theory both these oxidation states are highly unstable. Hence the dopant Mn^{2+} ion detraps the charge carriers to the surface adsorbed species to retain its stable electronic configuration [23–25].

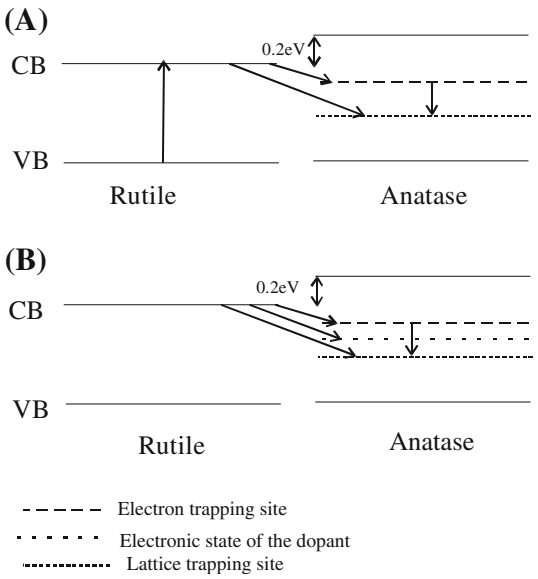

Fig. 4 Charge transfer in mixed phase. **a** In Degussa P-25 (taken from the reference [22]). **b** In T3

$$Mn^{2+} + e^{-} \rightarrow Mn^{+} \quad (2)$$

$$Mn^{+} + O_{2ads} \rightarrow Mn^{2+} + O_2^{-\bullet} \quad (3)$$

$$Mn^{2+} + h^{+} \rightarrow Mn^{3+} \quad (4)$$

$$Mn^{3+} + OH^{-} \rightarrow Mn^{2+} + OH^{\bullet} \quad (5)$$

Other possible mechanism can be that Mn^{+} can trap valence band holes or Mn^{3+} can trap conduction band electrons to retain its stable half filled electronic configuration

$$Mn^{+} + h^{+} \rightarrow Mn^{2+} \quad (6)$$

$$Mn^{3+} + e^{-} \rightarrow Mn^{2+} \quad (7)$$

This process accelerates the interfacial charge transfer process at the expense of recombination and also generates highly oxidative free radicals like hydroxyl and superoxide radicals which are most essential for oxidative degradation.

The transfer of electron from rutile to anatase has an activation barrier of 8.3×10^{-4} eV based on the measured rate of electron transfer [22]. Due to the low activation barrier, the effective inter particle electron transfer between the two polymorphs is quite possible only when they are in close proximity. The intimate contact between the two polymorphs depends mainly on their crystallite size. Hong et al. prepared iodine-doped titania which showed mixed phases of anatase and rutile after calcining the sample at 500 °C, which showed lower activity compared to iodine-doped anatase TiO_2. The low performance was accounted to the large rutile crystal size which resulted in poor intimate contact between these two phases which lacks to demonstrate its structure advantage [26]. Hence it is crucial to maintain the crystallite size of both the phases which enables the mixed phase for efficient charge transfer. P25 has anatase to rutile ratio of 80:20 with rutile crystallite (23 nm) slightly larger than anatase crystallite (20.3 nm). The sample T3 has anatase to rutile ratio of 90:10 and the crystallite size is 20.3 nm for both the phases. Since the crystallite size of both the phases is same, it can be speculated that both the polymorphs are in intimate contact in T3 compared to P25. According to Gray's results, such an interfacial mixed polymorph structure would contain a surplus amount of tetrahedral Ti^{4+} sites which can act as reactive electron-trapping sites [27]. These isolated tetrahedral Ti^{4+} sites are more active than octahedrally coordinated Ti^{4+} sites. The tetrahedral Ti^{4+} sites could serve as catalytic hot spots at anatase/rutile interface and thus avails the mixed polymorph nanocrystals into an effective photocatalytic relay for solar energy utilization. Hence we believe that these tetrahedral Ti^{4+} sites contribute to the increased activity of the mixed phase relative to the pure anatase/rutile phase.

The small crystallite size in T3 reduces the diffusion path length for the charge carriers, from the site where they are photo generated to the site where they react. Reduction in this diffusion path length results in lower recombination of charge carriers accelerating the interfacial charge transfer process. Therefore such an intimate contact between the mixed polymorph with smaller crystallites will have an core of rutile crystallites interwoven with bound anatase crystallites, thus accelerating the transfer of electrons from rutile to neighbouring anatase sites or to the impurity level created by the dopant. However it is vital that the existence of synergistic effect between the mixed polymorphs is not universal and there exist an optimum value for both the phases to show enhanced activity. In the present study, optimum value for anatase-to-rutile ratio was found to be 90:10. The induced oxygen vacancies by the Mn^{2+} dopant in the TiO_2 matrix and the other defects could become the centres to capture photoinduced electrons so that recombination of photo induced electrons and holes could be effectively inhibited. Thus the crystallite size, high intimate contact between the mixed phases and shallow trapping of Mn^{2+} results in enhanced activity of T3 compared to P25. In addition, T3 has the absorption band gap at 454 nm which absorbs more number of visible light photons compared to P25 which has absorption band edge nearly at 420 nm.

With the dopant concentration around 0.1% for T4, the crystallite size for both the phases is found to be 16.6 nm. In these crystallites most of the charge carriers are generated sufficiently close to the surface. As a result, the photo generated charge carriers may quickly reach the surface resulting in faster surface recombination reaction. This is also due to the excess trapping sites in the sample and lack of driving force to separate these charge carriers. In the catalyst with smaller crystallite size, surface charge carrier recombination reaction will be much faster than interfacial charge transfer process. Since Mn^{2+} serves as trapping site for both electron and hole, the possibilities of trapping both the charge carriers will be high at higher dopant concentration and this trapped charge carrier may recombine through quantum tunnelling [28]. Therefore there is a need for optimal dopant concentration in the TiO_2 matrix to get effective crystallite size for highest photocatalytic efficiency. Beyond the optimum dopant concentration, the rate of recombination starts dominating the reaction [24, 29] in accordance with the Eq. 8

$$K_{RR} \propto \exp(-2R/a_0) \tag{8}$$

Where K_{RR} is the rate of recombination, R is the distance separating the electrons and hole pairs, a_0 is the hydrogenic radius of the wave function for the charge carrier. As a consequence the recombination rate increases exponentially with the dopant concentration because the average distance between the trap sites decreases with increasing number of dopant ions confined with in a domain. Further it is suggested that Ti^{4+} in the TiO_2 with higher fraction of rutile is more difficult to be reduced to Ti^{3+} which suggests that trapping sites might serve as recombination centres which is in good agreement with Eq. 8 [8]. From the Fig. 3, it is shown that the plot follows first order kinetics for the samples T2 and T3 during the entire illumination time, while for the sample T4 it follows zero order kinetics after 15 min, suggesting that recombination of charge carriers dominates in these reactions [25].

The sample T3 with higher efficiency was chosen as a catalyst to study the photoelectro catalysis. The potential applied in the study are positive to the flat band potential of TiO_2 (≈ -0.38 V) [30]. The degradation efficiency increased as a function of applied potential up to +0.1 V for T3 ($k = 2.04\ min^{-1}$). Further increase in the potential results in slight decrease of degradation rate. The potential gradient over TiO_2 in the presence of applied field keeps the photo generated electron hole pair apart and as a result rate of recombination decreases. The effective separation of charge carriers in the presence of electric field increases the accumulation of electrons in the conduction band of rutile which consequently leads to surface band bending. This band bending facilitates the transfer of electrons between the mixed phases. The higher electric field existing in the space charge region favours the separation of photogenerated electron-hole pairs and hence increases photocatalytic activity. The photogenerated holes react with surface adsorbed water molecules to generate hydroxyl radicals. This hydroxyl radical reacts with benzene to yield hydroxylated derivatives and subsequent reaction of these intermediates results in complete degradation of the molecule. With increase in the applied bias to +0.2 V, the surface barrier becomes higher and the space charge region becomes very narrow and the penetration depth of light

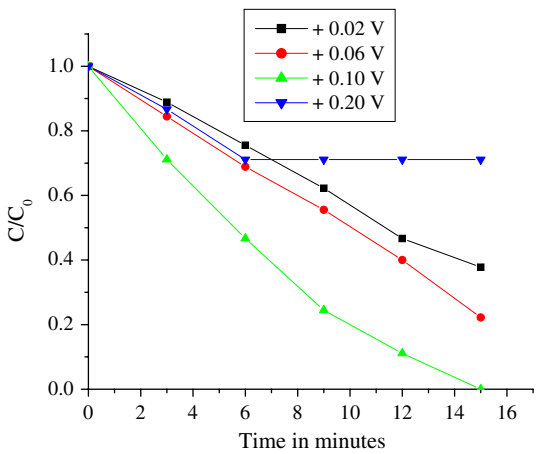

Fig. 5 Plot of C/C_0 versus time for the degradation of benzene under solar light using T3 as photocatalyst under various applied potentials

into the semiconductor lattice greatly exceeds the barrier width. Thus the fraction of incident light generates charge carriers in the bulk of the semiconductor which is field free. This facilitates the recombination which accounts for observed lower activity at higher applied potentials. The plot of C/C0 versus time for various applied potentials is depicted in Fig. 5. The results suggest that the degradation reaction follows first order kinetics up to the optimum potential and then follows zero order kinetics at higher potentials.

Acknowledgments Financial assistance from UGC Major Research Project (2007–2010), Government of India is acknowledged. The author Nagaraju Kottam acknowledges to M. S. Ramaiah institute of Technology for their support.

References

1. Devi LG, Krishnaiah GM (1999) J Photochem Photobiol A: Chem 121:141
2. Devi LG, Murthy BN (2008) Catal Lett 125:320
3. LG Devi, BN Murthy and SG Kumar (2009) Catal Lett. doi: 10.1017/s10562-009-9938-6
4. Devi LG, Kumar SG, Murthy BN, Kottam N (2009) Catal Commun 10:794
5. Chao HE, Yun YU, Xingfang HU, Larbot A (2003) J Eur Ceram Soc 23:1457
6. Huang Y, Zheng Z, Ai Z, Zhang L, Fan X, Zou Z (2003) J Phys Chem B 110:19323
7. Burns A, Hayes G, Li W, Hirvonen J, Demaree JD, Shan SI (2004) Mater Sci Eng B 111:150
8. Panpranot J, Kontapakdee K, Praserthdam P (2006) J Phys Chem B 110:8019
9. Meulen TVD, Mattson A, Osterlund L (2007) J Catal 251:131
10. Basca RR, Kiwi J (1998) Appl Catal B: Environ 16:19
11. Jun W, Gang Z, Zhaohong Z, Xiangdong Z, Guan Z, Teng M, Yuefeng J, Peng Z, Ying L (2007) Dyes Pigments 75:335
12. Lei S, Duan W (2008) J Environ Sci 20:1263
13. Ohno T, Sarukawa K, Tokieda K, Matsumura M (2000) J Catal 203:82
14. Ohno T, Tokieda K, Higashida S, matsumura M (2003) Appl Catal B: Environ 244:383
15. Lopez T, Gomez R, Sanchez E, Tzompantzi F, Vera L (2001) J Sol-Gel Sci Technol 22:99
16. Zhang Q, Gao L, Guo J (2000) Appl Catal B: Environ 26:207
17. Jung KY, Park SB, Jang HD (2006) Catal Commun 5:491
18. Bessekhouad Y, Robert D, Weber JV (2003) J Photochem Photobiol A: Chem 157:47
19. Slamet, Nasution HW, Purnama E, Kosela S, Gunlazuardi J (2005) Catal Commun 6:313–319
20. Xiao Q, Si Z, Yu Z, Qiu G (2007) Mater Sci Eng B 137:189
21. Leytner S, Hupp JT (2000) Chem Phys Lett 330:231
22. Hurum DC, Agrios AG, Gray KA, Rajh T, Thurnauer MC (2003) J Phys Chem B 107:4545
23. Yu J, Zhou M, Cheng B (2006) J Hazard Mater 137:1838
24. Choi W, Termin A, Hoffmann MR (1994) J Phys Chem 98:13669
25. Xu AW, Gao Y, Liu HQ (2002) J Catal 207:151
26. Hong X, Wang Z, Cai W, Lu F, Zhang J, Yang Y, Ma N, Lin Y (2005) Chem Mater 17:1548
27. Li G, Dimitrijevic NM, Chen L, Nichols JM, Rajh T, Gray KA (2008) J Am Chem Soc 130:5402
28. Zhang Z, Wang CC, Zakaria R, Ying JY (1998) J Phys Chem B 102:10871
29. Yang Y, Li XJ, Chen JT, Wang LY (2004) J Photochem Photobiol A: Chem 163:517
30. Zanoni MVB, Sene JJ, Anderson MA (2003) J Photochem Photobiol A: Chem 157:55